Regulation of Benzo[*a*]pyrene-Mediated DNA- and Glutathione-Adduct Formation by 2,3,7,8-Tetrachlorodibenzo-*p*-dioxin in Human Lung Cells

Stacy L. Gelhaus,[†,‡] Ronald G. Harvey,[§] Trevor M. Penning,[‡] and Ian A. Blair*[,†,‡]

Center for Cancer Pharmacology and Center for Excellence in Environmental Toxicology, University of Pennsylvania, Philadelphia, Pennsylvania 19104-6610, United States, and The Ben May Department for Cancer Research 3, University of Chicago, Chicago, Illinois 60637, United States

Received August 31, 2010

Environmental carcinogens, such as polycyclic aromatic hydrocarbons (PAHs), require metabolic activation to DNA-reactive metabolites in order to exert their tumorigenic effects. Benzo[*a*]pyrene (B[*a*]P), a prototypic PAH, is metabolized by cytochrome P450 (P450) 1A1/1B1 and epoxide hydrolase to (−)-B[*a*]P-7,8-dihydro-7,8-diol (B[*a*]P-7,8-dihydrodiol). B[*a*]P-7,8-dihydrodiol then undergoes further P4501A1/1B1-mediated metabolism to the ultimate carcinogen, (+)-*anti*-7,8-dihydroxy-9,10-epoxy-7,8,9,10-tetrahydro-B[*a*]P (B[*a*]PDE), which forms DNA-adducts primarily with 2′-deoxyguanosine (dGuo) to form (+)-*anti-trans*-B[*a*]PDE-N^2-dGuo (B[*a*]PDE-dGuo) in DNA. Pretreatment of cells with 2,3,7,8-tetrachlorodibenzo-*p*-dioxin (TCDD) is known to induce P4501A1/1B1 mRNA expression through the aryl hydrocarbon receptor (AhR) pathway. This causes increased B[*a*]PDE-dGuo formation in liver cells. In contrast, TCDD induction of H358 lung cells surprisingly caused a decrease in (−)-B[*a*]P-7,8-dihydrodiol-mediated (+)-B[*a*]PDE-dGuo adduct formation when compared with the non-TCDD-induced cells. Furthermore, treatment of the TCDD-induced cells with (±)-B[*a*]PDE also resulted in decreased (+)-B[*a*]PDE-dGuo adduct formation when compared with the non-TCDD-induced cells. These data suggested that it was a detoxification pathway that had been up-regulated rather than an activation pathway that had been down-regulated. LC-MS was used to analyze B[*a*]PDE-dGuo and B[*a*]PDE-GSH-adducts in H358 lung and HepG2 liver cells. There was a significant increase in the (−)-B[*a*]PDE-GSH-adduct with high enantiomeric excess after treatment of the TCDD-induced H358 cells with (±)-B[*a*]PDE when compared with the noninduced cells. This could explain why increased activation of (−)-B[*a*]P-7,8-dihydrodiol through TCDD up-regulation of P4501A1/1B1 did not lead to increased (+)-B[*a*]PDE-dGuo adducts in the H358 lung cells. In addition, TCDD did not induce B[*a*]PDE-GSH-adduct formation in HepG2 liver cells. (±)-B[*a*]PDE-GSH-adducts were formed at much lower levels in both TCDD-induced and noninduced HepG2 cells when compared with (−)-B[*a*]PDE-GSH-adducts in the H358 lung cells. Therefore, our study has revealed that there is a subtle balance between activation and detoxification of B[*a*]P in lung-derived compared with liver-derived cells and that this determines how much DNA damage occurs.

Introduction

Polycyclic aromatic hydrocarbons (PAHs[1]) are ubiquitous environmental pollutants. They are formed through the combustion of coal, oil, gas, wood, garbage, or other organic substances, including tobacco and charbroiled meat (*1*−*4*). Exposure to PAHs occurs primarily through environmental pollutants including mainstream and sidestream smoke, as well as car exhaust emissions (*5*). In smokers, B[*a*]P levels range from 0.5 to 7.8 μg/100 cigarettes when exposure is from mainstream smoke and from 2.5 to 19.9 μg/100 cigarettes from side-stream smoke (*6*). Nonsmokers are exposed to PAHs through passive smoking, although at much lower levels of 0.003 to 0.760 $\mu g/m^3$ (*6*). In addition, both smokers and nonsmokers are exposed to PAHs through the diet and indoor/outdoor air (*5, 7, 8*). PAHs reaching the lung and the systemic circulation can be activated to reactive metabolites (*7, 8*), which are detoxified and excreted from the body (*9, 10*). However, when the detoxification pathways are saturated (*11*), the reactive metabolites can directly and covalently modify DNA to form DNA-adducts or produce reactive oxygen species that cause oxidative DNA damage (*4, 12*). There is substantial evidence to suggest that PAHs are causative agents in lung (*13, 14*), skin (*15, 16*), and bladder cancers (*15, 16*). Numerous previous reports have linked B[*a*]P exposure with DNA-adduct formation, which then results in genetic alterations that contribute to the development of multistage carcinogenesis. For example, B[*a*]P-adduct formation has been shown to

* To whom correspondence should be addressed. Center for Cancer Pharmacology, University of Pennsylvania School of Medicine, 854 BRB II/III, 421 Curie Boulevard, Philadelphia PA 19104-6160.

† Center for Cancer Pharmacology, University of Pennsylvania.

‡ Center for Excellence in Environmental Toxicology, University of Pennsylvania.

§ University of Chicago.

[1] Abbreviations: AhR, aryl hydrocarbon receptor; AKR, aldo-keto reductase; ARE, antioxidant response element; B[*a*]P, benzo[*a*]pyrene; B[*a*]PDE, (±)-*anti*-7,8-dihydroxy-9,10-epoxy-7,8,9,10-tetrahydro-B[*a*]P; (+)-B[*a*]PDE-dGuo, (+)-*anti-trans*-B[*a*]P-7,8-diol-9,10-epoxide-2′-deoxyguanosine; B[*a*]PDE-GSH-adduct, (±)-*anti*-B[*a*]PDE-GSH-adduct; (−)-B[*a*]P−7,8-dihydrodiol, (−)-*trans*-7,8-dihydroxy-7,8-dihydro-benzo[*a*]pyrene; B[*a*]P-7,8-dione, benzo[*a*]pyrene-7,8-dione; CID, collision induced dissociation; FBS, fetal bovine serum; GST, glutathione-*S*-transferase; LC-ESI/MRM/MS, LC-electrospray ionization/multiple reaction monitoring/MS; PAH, polycyclic aromatic hydrocarbon; RPMI 1640, Roswell Park Memorial Institute 1640; TCDD, 2,3,7,8-tetrachlorodibenzo-*p*-dioxin; XRE, xenobiotic response element.

10.1021/tx100297z
Published on Web 10/28/2010

Scheme 1. Metabolism of B[*a*]P in Human Lung Cells

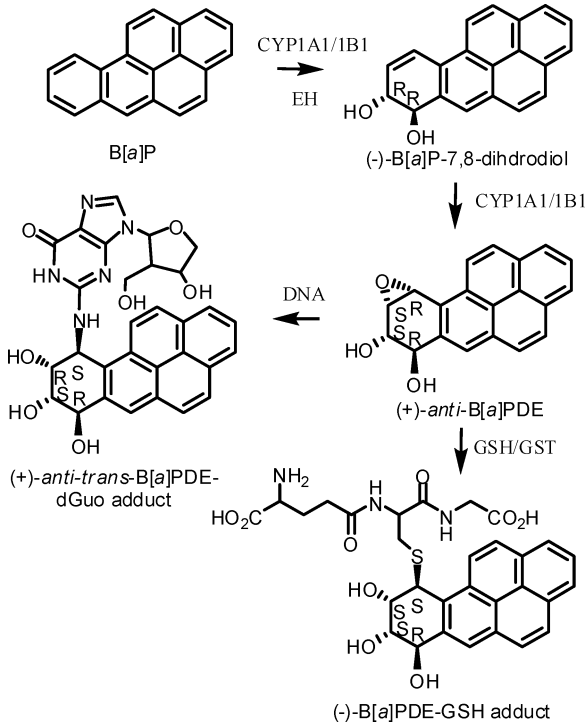

inactivate the tumor suppressor, p53, by covalent DNA-adduct formation on guanine bases in the DNA-binding domain (*17*).

Several pathways of B[*a*]P activation are known to be important (*4*). However, P4501A1/1B1-mediated activation is the most widely accepted pathway for the formation of B[*a*]P-derived DNA-adducts (*4*). B[*a*]P is oxidized initially by P4501A1/1B1, to B[*a*]P-7,8-oxide, which undergoes epoxide hydrolase (EH)-mediated hydrolysis to the proximate carcinogen (−)-B[*a*]P-7,8-dihydro-7,8-diol (B[*a*]P-7,8-dihydrodiol) (*7, 8*). P4501A1 and 1B1 are considered to be the major P450s involved in the activation of B[*a*]P (*18, 19*). Other human P450s (including P450s 1A2, 2E1, and 3A4) have very low or undetectable activities toward the formation B[*a*]P-7,8-dihydrodiol (*18*). Further activation of (−)-B[*a*]P-7,8-dihydrodiol occurs through P4501A1/1B1-mediated metabolism to (+)-B[*a*]PDE, the ultimate carcinogenic reactive metabolite (*20*). Other isoforms, including P4501A2, are able to metabolize B[*a*]P-7,8-dihydrodiol to B[*a*]PDE to a lesser degree (*20*). (+)-B[*a*]PDE can be detoxified through glutathione *S*-transferase (GST)-mediated GSH-adduct formation (*21, 22*) or through further hydrolysis to the corresponding tetraols (*23*). B[*a*]PDE that escapes detoxification reacts with DNA to form adducts, primarily at the exocyclic N^2-amine of dGuo (*24*). In our previous study, H358 lung cells were treated with (±)-B[*a*]P-7,8-dihydrodiol, and the amount of each (±)-B[*a*]PDE-derived DNA-adduct was quantified (*4*). The dGuo- and 2′-deoxyadenosine (dAdo)-adduct formation in the P450/AKR expressing cells was then compared to adduct formation from B[*a*]P, (−)-B[*a*]P-7,8-dihydrodiol, and (+)-B[*a*]P-7,8-dihydrodiol treatment. These studies revealed that (+)-B[*a*]PDE-dGuo was the major adduct and that in contrast to liver cells, its formation was maximal in H358 lung cells that had not been induced with TCDD (Scheme 1) (*4*).

In order to further elucidate the mechanism underlying this paradoxical effect, we have conducted experiments to examine the dose−response of DNA-adduct formation to (−)-B[*a*]P-7,8-dihydrodiol and TCDD in H358 cells. In addition, a microarray analysis was conducted with H358 lung cells that had been treated with (−)-B[*a*]P-7,8-dihydrodiol and/or TCDD. (±)-B[*a*]PDE-derived GSH-adducts were analyzed in the (±)-B[*a*]PDE-treated TCDD-induced H358 cells to determine whether there was increased GSH-adduct formation compared with that in the noninduced cells. Finally, the levels of B[*a*]PDE-derived GSH-adducts in H358 cells and media were compared to levels in human liver carcinoma, HepG2, cells and media with and without TCDD induction. Total GST activity was also measured in H358 and HepG2 noninduced and TCDD-induced cells.

Materials and Methods

Caution: *All PAHs are potentially hazardous and should be handled in accordance with NIH Guidelines for the Use of Chemical Carcinogens.*

Materials and Reagents. H358 and HepG2 cells were purchased from the American Tissue Culture Collection (ATCC; Manassas, VA). Cell culture medium and reagents were all obtained from Invitrogen Co. (Carlsbad, CA) except for fetal bovine serum, which was from (FBS) Hyclone (Logan, Utah). (−)-B[*a*]P-7,8-dihydrodiol, (±)-B[*a*]PDE, and TCDD were obtained from NCI Chemical Carcinogen Standard Reference Repository (Midwest Research Institute, Kansas City, Missouri). Equine GST, dGuo, dAdo, and Me_2SO were purchased from Sigma Aldrich (St. Louis, MO). [$^{15}N_5$]-2′-dGuo was purchased from Cambridge Isotope Laboratories (Andover, MA). [$^{15}N_5$]-B[*a*]PDE-dGuo was synthesized as described previously (*24*), and the [$^{13}C_2$]-B[*a*]P-7,8-dihydrodiol internal standard was synthesized by Dr. R. Harvey. The purity and identity of all B[*a*]P metabolites was established by LC-MS as previously described (*24, 25*). Ammonium acetate and formic acid were HPLC grade, and the methanol was Optima grade (Fisher Scientific, Waltham, MA). All water was purified through a Milli-Q reverse osmosis system (Millipore, Billerica, MA).

Preparation of Authentic (±)-B[*a*]PDE-GSH-Adducts. The GSH-adducts were prepared by a modification of the method described previously (*25*). Briefly, (±)-B[*a*]PDE (200 μg) was incubated for 1 h with equine GST (100 units) and GSH (4 mM) in 100 mM potassium phosphate buffer (pH 6.5) at 37 °C. The (−)-B[*a*]PDE-GSH-adduct eluted at an earlier retention time than the (+)-B[*a*]PDE-GSH-adduct on the YMC ODS-AQ column under the conditions described below. This is similar to the elution profile described previously (*26*). Product ion spectra from collision-induced dissociation (CID) of *m/z* 610 (B[*a*]PDE-GSH, MH^+) were essentially identical for the two enantiomers: *m/z* 592 (MH^+-H_2O), *m/z* 574 (MH^+-$2H_2O$), *m/z* 445 (MH^+-H_2O-ã-Glu), *m/z* 427 (MH^+-$2H_2O$-ãGlu), *m/z* 308 (GSH+H^+), *m/z* 303 (B[*a*]PDE+H^+), *m/z* 285 (B[*a*]PDE+H^+-H_2O), and *m/z* 257(B[*a*]PDE+H^+-H_2O−CO).

Cell Culture. Human bronchoalveolar H358 cells (ATCC #CRL-5807) were maintained in RPMI 1640 nutrient mixture with 10% heat-inactivated FBS, 2 mM L-glutamine, 100 units/mL penicillin, and 100 μg/mL streptomycin. Human liver carcinoma HepG2 cells (ATCC #HB-8065) were maintained in Eagle's Minimum Essential Medium with 10% heat-inactivated FBS, 100 units/mL penicillin, and 100 μg/mL streptomycin. Cells were incubated at 37 °C in a humidified atmosphere containing 5% CO_2 and were passaged every 3 days at a 1:3 dilution. Cultured cells with a passage number of 15 or less were used in the experiments to reduce variability during cell culture.

(−)-B[*a*]P-7,8-Dihydrodiol Concentration Dependence. Control, untreated H358 cells and TCDD-induced (10 nM, 24 h) H358 cells were treated with increasing concentrations of (−)-B[*a*]P-7,8-dihydrodiol in 0.3% Me_2SO (0.1 μM to 2 μM) or 0.3% Me_2SO for 24 h. The (+)-B[*a*]PDE-dGuo and total DNA were then quantified as described below.

(−)-B[*a*]P-7,8-Dihydrodiol Metabolism. H358 cells were treated with 2 μM (−)-B[*a*]P-7,8-dihydrodiol in 0.3% Me_2SO for 6 h with and without 10 nM TCDD pretreatment in 10 mL of RPMI/FBS medium. At 6 h, cells were collected, and the remaining (−)-B[*a*]P-7,8-dihydrodiol was analyzed as described below.

TCDD Concentration Dependence for (−)-B[*a*]P-7,8-Dihydrodiol-Mediated DNA-Adduct Formation. H358 cells (10^6/cells plate) were pretreated in 10 mL of RPMI/FBS medium with increasing concentrations of TCDD (0, 1, 10 nM) for 24 h before treatment with (−)-B[*a*]P-7,8-dihydrodiol (5.7 μg, 2 μM final concentration) in 0.3% Me_2SO for 24 h. The (+)-B[*a*]PDE-dGuo and total DNA were then quantified as described below.

(±)-B[*a*]PDE and TCDD Treatment. H358 cells (10^6/cells plate) were treated in 10 mL RPMI/FBS medium with 2 μM (±)-B[*a*]PDE (6.1 μg, 2 μM final concentration) in 0.3% Me_2SO (24 h) with or without TCDD (10 nM) pretreatment for 24 h. The (+)-B[*a*]PDE-dGuo and total DNA were then quantified as described below. Additionally, H358 and HepG2 cells (2×10^5/cells plate) were treated in 2 mL of media with (±)-B[*a*]PDE (12.1 μg, 20 μM final concentration) in 0.3% Me_2SO (30 min, 1, 2, 4, and 6 h) with and without TCDD (10 nM) pretreatment for 24 h. Cells and media were collected, and two plates were combined into one sample for the measurement of B[*a*]PDE-GSH-adducts by LC-ESI-MS/MS as described below.

LC-ESI/MRM/MS. Data for (+)-B[*a*]PDE-dGuo adducts were acquired using an Agilent 1100 HPLC system (Agilent Technology, Palo Alto, CA) equipped with a CTC autosampler (Leap Technology, Carrboro, NC) and an MDS-Sciex API-4000 triple-quadrupole mass spectrometer (Applied Biosystems, Foster City, CA). The HPLC method employed a YMC J'sphere M80 column (2.0 mm I.D. × 150 mm, 4 μm) using 5 mM NH_4OAc buffer containing 0.02% formic acid as mobile phase A and methanol as mobile phase B at a flow rate of 200 μL/min. The gradient started from 49% B to 51% B in 20 min, followed by 51% B to 65% B in 10 min, and continued to 100% B in 5 min. The following mass spectrometer parameters were set: collision gas (nitrogen), 10 units; curtain gas (nitrogen), 30 units; ion source gas number 1 (nitrogen), 30 units; ion source gas number 2 (nitrogen), 30 units; ion spray voltage, 5.0 kV; ionization temperature, 500 °C; decluster potential, 50 V; entrance potential, 8 V; collision energy, 40 eV; and collision cell exit potential, 22 V. MRM analyses were conducted in positive ESI mode. The following transitions were monitored for (+)-B[*a*]PDE-dGuo: *m/z* 570.2 (MH^+, (+)-B[*a*]PDE-dGuo) → *m/z* 257.1 (MH^+-dGuo-H_2O-CO) and *m/z* 575.2 ([$^{15}N_5$]-B[*a*]PDE-dGuo) → *m/z* 257.1 (MH^+-[$^{15}N_5$]-dGuo-H_2O-CO).

Data for (−)-B[*a*]P-7,8-dihydrodiol were also acquired using the instrumentation described above. The HPLC method employed a Phenomenex Luna C18(2)-ODS column (4.0 mm I.D. × 125 mm, 4 μm) using 5 mM NH_4OAc buffer containing 0.1% formic acid as mobile phase A and methanol containing 0.1% formic acid as mobile phase B at a flow rate of 300 μL/min. The gradient started from 60% B to 70% B in 20 min, followed by 70% B to 80% B in 10 min. This was held for 20 min followed by an increase to 95% B in 5 min. Again, this was held for 5 min before returning to starting 60% B, held for 20 min for column equilibration. Mass spectrometer parameters different from those used for (+)-B[*a*]PDE-dGuo adducts were collision gas, 9 units; curtain gas, 10 units; ion source gas number 2, 50 units; entrance potential, 12 V; collision energy, 30 eV; and collision cell exit potential, 20 V. The following transitions were monitored: for (−)-B[*a*]P-7,8-dihydrodiol, *m/z* 269.1 (MH^+-H_2O, (−)-B[*a*]P-7,8-dihydrodiol) → *m/z* 251.1 (MH^+-$2H_2O$); for [$^{13}C_2$]-(−)-B[*a*]P-7,8-dihydrodiol, *m/z* 271.3 (MH^+-H_2O), [$^{13}C_2$]- (−)-B[*a*]P-7,8-dihydrodiol) → *m/z* 253.3 (MH^+-$2H_2O$).

Data for the B[*a*]PDE-GSH-adduct were acquired using a Waters 2690 HPLC system (Waters Co., Milford, MA) equipped with an autosampler and a Thermo Fisher LTQ ion trap mass spectrometer (Thermo Fisher, Mullica Hill, NJ). The HPLC method employed a YMC ODS-AQ column (2.0 mm I.D. × 150 mm, 3 μm) using water containing 0.1% formic acid as mobile phase A and acetonitrile containing 0.1% formic acid as mobile phase B at a flow rate of 200 μL/min. The gradient started from 20% B to 50% B in 8 min, followed by 50% B to 100% B in 14 min; 100% B was held for 3 min followed by a return to starting conditions, 20% B for 10 min. The following mass spectrometer parameters were set: nitrogen was used for sheath (41 units) and auxiliary gas (12 units). Helium was used as the collision gas with a collision energy of 35 eV. All analyses, full scans, product ion scans, and MRM were conducted in positive ESI mode. The following transition was monitored for the B[*a*]PDE-GSH-adduct: *m/z* 610.2 (MH^+, B[*a*]PDE-GSH) → *m/z* 308.1 (GSH+H^+).

Microarray Analysis. H358 cells ($n = 6$ for each treatment group) were treated with the Me_2SO vehicle control for 48 h, 10 nM TCDD for 48 h, 2 μM (−)-B[*a*]P-7,8-dihydrodiol for 24 h, or a combination of 10 nM TCDD and 2 μM (−)-B[*a*]P-7,8-dihydrodiol for 48 and 24 h, respectively. After the allotted treatment times, total RNA was extracted from H358 cells using the miRNeasy protocol from Qiagen. Microarray analysis was performed according to the Affymetrix protocol using the Affymetrix HuGene 1.0 array platform (Santa Clara, CA). Four samples from each treatment category were chosen for microarray analysis. Data analysis was performed using Partek Genomics Suite (Partek Inc., St. Louis, MO). Subsequent visualization and filtering used Spotfire DecisionSite, version 9.1 (Tibco Software Inc., Palo Alto, CA, USA). Affymetrix .cel files were imported, and Robust Multiarray Average was performed on the microarray data yielding $\log_2$ transformed signal intensities for each probeset on each array. Next, the low expression probesets were filtered out, retaining probesets with $\log_2$ intensities of greater than 5 in at least 3 of the 16 samples. This left 22,136 probesets available for statistical analysis. A one way ANOVA with 6 pairwise contrasts was then performed yielding *p*-values for the ANOVA and for each of the comparisons. Fold-change values for each of the pairwise comparisons were also calculated. The 6 comparisons included TCDD vs Me_2SO, diol vs Me_2SO, TCDD-diol vs Me_2SO, diol vs TCDD, and TCDD-diol vs TCDD and TCDD-diol vs diol. For each calculated *p*-value, a Benjamini−Hochberg step-up *p*-value was also determined to assess the false discovery rate.

Quantification of DNA-Adducts. For calibration curves of the DNA-adducts, the four stereoisomers of authentic B[*a*]PDE-N^2-dGuo and B[*a*]PDE-[$^{15}N_5$]-N^2-dGuo were used to make standard mixtures of different concentrations (0.1, 0.2, 0.5, 1.0, 2.5, 5.0, and 10.0 ng of each). The standard solutions underwent the same sample preparation and analytical procedures as the experimental samples described above. Calibration curves were calculated with a linear regression analysis of the peak area ratios of standard versus the internal standard. DNA-adduct levels were calculated by interpolation from the calibration curve and normalized with the total base content in each sample (*4*). Levels are reported as number of (+)-B[*a*]PDE-dGuo adducts per 10^6 normal bases.

DNA Base Analysis. LC-UV chromatography for DNA base analysis was conducted on a Hitachi Elite Lachrom HPLC system equipped with a UV detector. The separation employed a Phenomenex Luna C18(2) column (4.0 mm I.D. × 125 mm, 5 μm). Solvent A was aqueous 5 mM NH_4OAc with 0.02% formic acid, and solvent B was methanol. The flow rate was 0.9 mL/min, and DNA bases were separated isocratically at 15% B for 20 min. The UV detector monitored the absorbance at 260 nm. For calibration curves, solutions containing certain concentrations of authentic DNA bases (0.0, 2.0, 5.0, 10.0, 20.0, and 50.0 μg/mL) were subjected to HPLC-UV analysis. The injection volume was 20 μL. Calibration curves were calculated with a linear regression analysis of the peak areas of authentic standards. A portion of the digested sample was subjected to the same HPLC-UV procedure for base analysis. The DNA base level was calculated by interpolation from the calibration curve.

GST Activity Assay. The activity of total GST was assessed in TCDD-induced and noninduced H358 and HepG2 cells using 1-chloro,2,4-dinitrobenzene (CDNB). Induced H358 and HepG2 cells were treated with 10 nM TCDD for 24 h. Briefly, 0.1 M KH_2PO_4, pH 6.5, 1.0 mM CDNB, 1.0 mM GSH-, and either GSTα-1 (1 μg) or cell lysate (25 μL) were then combined. Total GST activity was assessed by monitoring CDNB-GSH-adduct formation at 340 nm over 15 min, during which time adduct formation was linear. Activity is reported in nmol/min/mg protein, and nonenzymatic GSH-adduct formation was taken into account

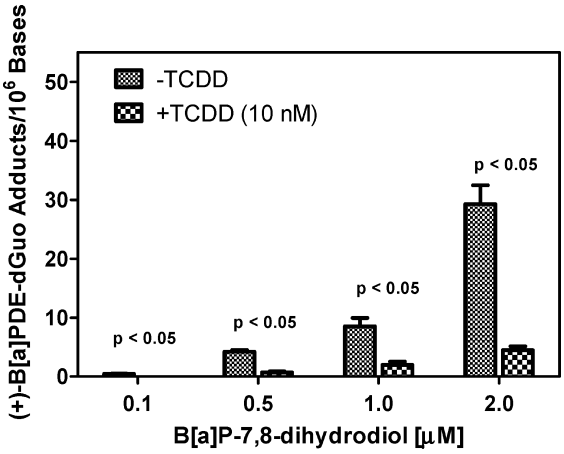

Figure 1. (−)-B[*a*]P-7,8-dihydrodiol concentration dependence. The levels of (+)-B[*a*]PDE-dGuo DNA-adducts formed in H358 cells with increasing concentrations of (−)-B[a]P-7,8-diol (0.1, 0.5, 1.0, and 2.0 μM) in 24 h with and without 10 nM TCDD pretreatment for 24 h. Experiments were conducted in triplicate, and the values are expressed as the means ± SEM. B[*a*]PDE-dGuo levels were significantly higher ($p < 0.05$) in H358 cells not treated with TCDD.

by quantifying CDNB-GSH adduct formation in controls that included everything except the enzyme.

Results

TCDD Effect on (−)-B[*a*]P-7,8-Dihydrodiol-Mediated DNA-Adduct Formation in Lung Cells. H358 cells were pretreated with 10 nM TCDD for 24 h before (−)-B[*a*]P-7,8-dihydrodiol treatment for 24 h. At the lowest concentration of 0.1 μM (−)-B[*a*]P-7,8-dihydrodiol, (+)-B[*a*]PDE-dGuo-adduct levels were below the limit of detection of 10 pg on column (Figure 1)), which was rigorously determined in our previous study (*24*). The TCDD caused a significant decrease in (+)-B[*a*]PDE-dGuo adducts at each concentration of (−)-B[*a*]P-7,8-dihydrodiol that was used. There was almost a 7-fold decrease of (+)-B[*a*]PDE-dGuo adducts at 2 μM (−)-B[*a*]P-7,8-dihydrodiol, the highest concentration that was examined (Figure 1). There was also significant up-regulation ($p < 0.05$) of GSTM1 (1.3-fold), ALDH3A1 (2-fold), and ALDH1A3 (2.8-fold). The increase in CYP1A1 mRNA detected by the microarray experiments was validated by quantitative PCR using CYP1A2 as a negative control (data not shown).

(−)-B[*a*]P-7,8-Dihydrodiol Metabolism. Residual (−)-B[*a*]P-7,8-dihydrodiol was detected in the cells by LC-MRM/MS after 6 h when 2 μM (−)-B[*a*]P-7,8-dihydrodiol was used with and without 10 nM TCDD pretreatment for 24 h (Figure 2). Quantitation using the [$^{13}C_2$]-(−)-B[*a*]P-7,8-dihydrodiol internal standard revealed that (−)-B[*a*]P-7,8-dihydrodiol was metabolized at a faster rate with TCDD induction.

Effect of TCDD Concentration on DNA-Adduct Formation. H358 cells were induced with different concentrations of TCDD (0, 1, and 10 nM) for 24 and then treated with 1.0 μM (−)-B[*a*]P-7,8-dihydrodiol for 24 h. There was significant reduction in (+)-B[*a*]PDE-dGuo adducts as the concentration of TCDD used in the induction was increased from 0 nM to 1 nM and from 1 nM to 10 nM (Figure 3).

Microarray Analysis of Lung Cells Treated with TCDD and B[*a*]P Metabolites. Significant effects on P4501A1 and P4501B1 mRNA expression were observed. None of the other genes that have been previously associated with B[*a*]P metabolism in the lung were significantly up- or down-regulated. Treatment of H358 cells with 10 nM TCDD for 48 h, resulted in a P4501A1 superinduction of 80-fold together with a

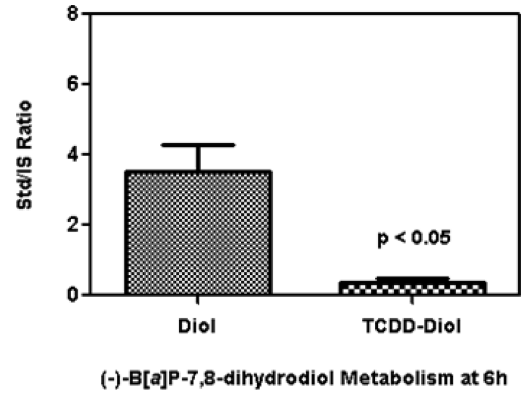

Figure 2. LC-MRM/MS analysis of (−)-B[*a*]P-7,8-dihydrodiol in H358 cells. Analyses were conducted after a 6 h incubation of H358 cells treated with 2 μM (−)-B[a]P-7,8-dihydrodiol with and without 10 nM TCDD pretreatment for 24 h. The ratio of (−)-B[*a*]P-7,8-dihydrodiol to the [$^{13}C_2$]-B[*a*]P-7,8-dihydrodiol internal standard was calculated for experiments in triplicate. Experiments were conducted in triplicate, and the values are expressed as the means ± SEM. The ratio for H358 cells pretreated with 10 nM TCDD for 24 h was significantly lower ($p < 0.05$) than that of H358 cells that were not pretreated with TCDD.

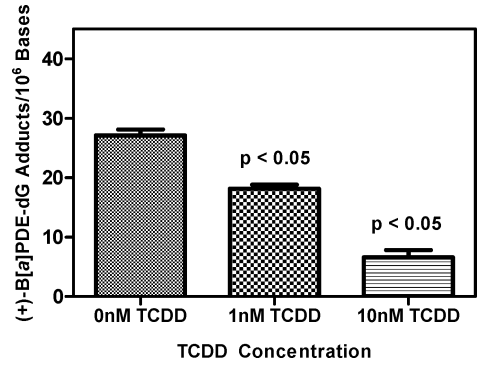

Figure 3. TCDD concentration dependence. H358 cells were pretreated with TCDD (0, 1.0, and 10 nM) for 24 h and treated with 1.0 μM (−)-B[*a*]P-7,8-dihydrodiol for 24 h. Experiments were conducted in triplicate, and the values are expressed as the means ± SEM. As the concentration of TCDD increased, the level of (+)-B[*a*]PDE-dGuo decreased significantly ($p < 0.05$).

substantial increase in P4501B1 mRNA (12-fold) (Figure 4). The effect on P4501A1 was attenuated by the addition of (−)-B[*a*]P-7,8-didhydrodiol for 24 h to a level similar to that observed with the (−)-B[*a*]P-7,8-dihydrodiol alone for 24 h (16-fold) (Figure 4). P4501B1 was induced 12-fold by TCDD treatment for 48 h. Addition of (−)-B[*a*]P-7,8-dihydrodiol alone induced P4501B1 mRNA expression 7-fold compared to that in the Me_2SO control. The addition of (−)-B[*a*]P-7,8-dihydrodiol after 24 h of TCDD treatment attenuated the effect of TCDD on CY1B1 and resulted in a 9-fold increase in P4501B1 mRNA levels compared to that in the Me_2SO control.

(±)-B[*a*]PDE-Mediated DNA-Adduct Formation in Lung Cells. H358 cells were treated with 2 μM (±)-B[*a*]PDE for 24 h. (+)-B[*a*]PDE-dGuo adduct levels were 13.5 ± 1.0 adducts/10^6 bases (Figure 5). TCDD pretreatment for 24 h resulted in a significant decrease in adduct formation ($p < 0.003$) to 6.0 ± 0.4 adducts/10^6 bases (Figure 5).

(±)-B[*a*]PDE-Mediated GSH-Adduct Formation in Lung and Liver Cells. LC-MS/MS analysis revealed an almost 10-fold increase in intracellular (−)-B[*a*]PDE GSH-adduct formation in the TCDD-induced H358 lung cells (Figure 6A; intensity 3.9×10^5) compared with that in the noninduced H358 cells (Figure 6C; intensity 4.3×10^4) after a 4 h incubation. The chromatographic peak observed at 12.4 min in Figure 6A and

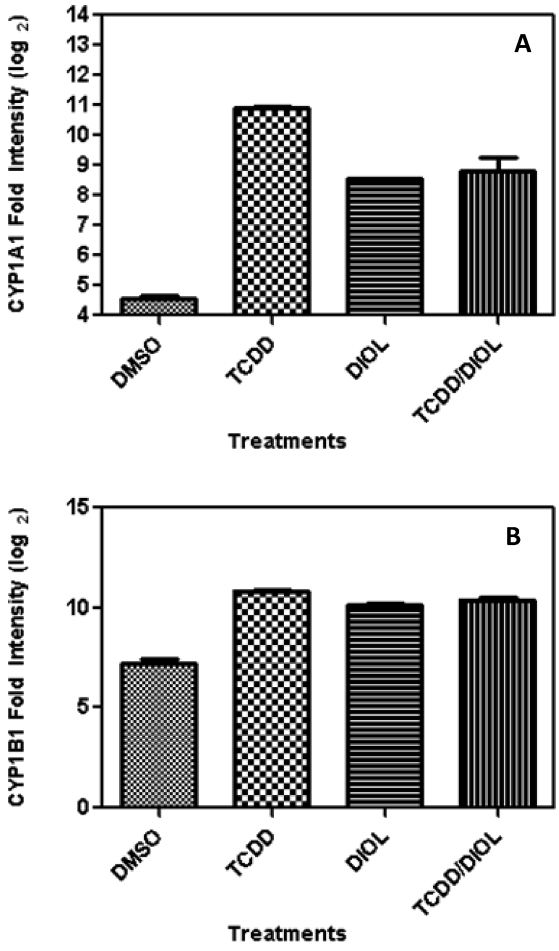

Figure 4. Microarray expression. The fold change in mRNA depending upon the various cell treatments: DMSO, 10 nM TCDD (48 h), 2 μM (−)-B[*a*]P-7,8-dihydrodiol (24 h), and 10 nM TCDD (48 h) with 2 μM (−)-B[*a*]P-7,8-dihydrodiol (24 h). (A) CYP1A1. (B) CYP1B1.

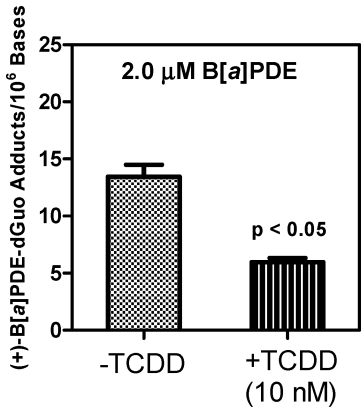

Figure 5. Measurement of (+)-B[*a*]PDE-dGuo H358 cells treated with 2 μM (±)-B[*a*]PDE with and without 10 nM TCDD pretreatment. (+)-B[*a*]PDE-dGuo formation with TCDD-induced cells was decreased compared with that of the noninduced cells.

B was not derived from a B[*a*]P-GSH-adduct and therefore did not appear in the corresponding LC-MRM/MS chromatogram (Figure 7A). The product ion spectrum of (−)-B[*a*]PDE-GSH-adduct (Figure 6B) was identical to that obtained from an authentic standard prepared using equine GST and (±)-B[*a*]PDE (data not shown). LC-MRM/MS analysis showed that intracellular (−)-B[*a*]PDE-GSH-adduct formation in TCDD-induced H358 lung cells was almost 2 orders of magnitude greater (Figure 7A; peak area 454,522) than (±)-B[*a*]PDE-GSH-adduct formation in TCDD-induced HepG2 liver cells (Figure 7C; total

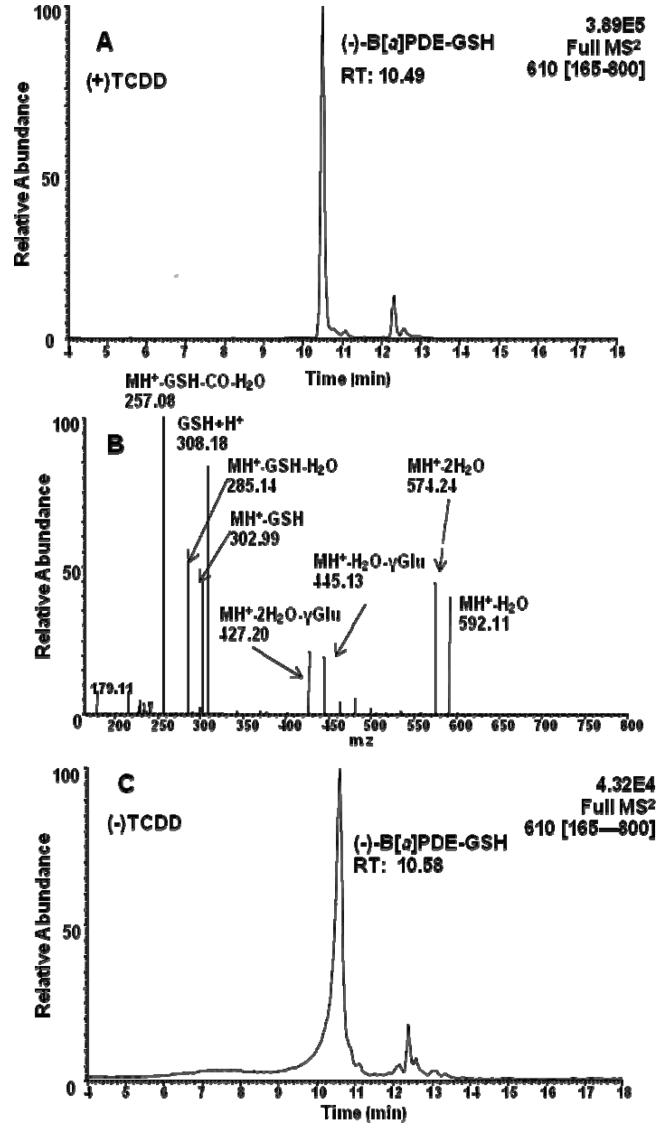

Figure 6. LC-MS/MS analysis of B[*a*]PDE-GSH-adducts in (±)-B[*a*]PDE-treated H358 cells. (A) LC-MS/MS chromatogram of the intracellular (−)-B[*a*]PDE-GSH-adduct in TCDD-induced H358 cells after a 4 h incubation. (B) Product ion spectrum of the (−)-B[*a*]PDE-GSH-adduct (MH^+, *m/z* 610) in TCDD-induced H358 cells. (C) LC-MS/MS chromatogram of the intracellular (−)-B[*a*]PDE-GSH-adduct in noninduced H358 cells after a 4 h incubation. H358 cells pretreated with 10 nM TCDD for 24 h had increased levels of (−)-B[*a*]PDE-GSH-adducts.

peak area 5,628) after a 4 h incubation. Furthermore, enantioselective formation of the (−)-B[*a*]PDE-GSH-adduct was observed in H358 cells (Figure 7A), whereas racemic (±)-B[*a*]PDE-derived GSH-adducts were formed in HepG2 cells (Figure 7C). The product ion spectra for the (−)-B[*a*]PDE-GSH-adduct (Figure 6B) and (+)-B[*a*]PDE-GSH-adduct (Figure 7B) were identical to the spectra from synthesized standards (data not shown).

LC-MRM/MS analyses conducted over a 6 h period revealed that intracellular and extracellular (−)-B[*a*]PDE-GSH-adducts were an order of magnitude higher at all time points in the TCDD-induced H358 lung cells (Figure 8A and B) when compared with that in the noninduced cells (Figure 9A and B). In contrast, there was virtually no difference over a 6 h period between intracellular and extracellular (±)-B[*a*]PDE-GSH-adducts in the TCDD-induced HepG2 liver cells (Figure 8C and D) when compared with the noninduced cells (Figure 9C and D). Therefore, TCDD induction caused an almost 2 orders

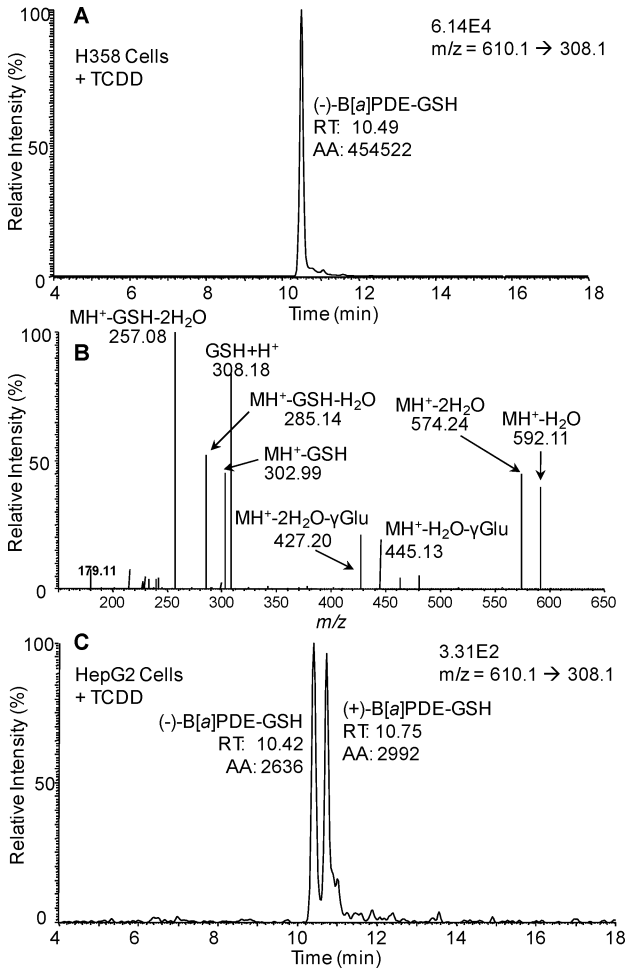

Figure 7. LC-MRM/MS analysis of B[*a*]PDE-GSH-adducts in (±)-B[*a*]PDE-treated H358 and HepG2 cells with 10 nM TCDD pretreatment for 24 h. (A) Intracellular (−)-B[*a*]PDE-GSH-adducts in TCDD-induced H358 cells after a 4 h incubation. (B) Product ion spectrum of the (+)-B[*a*]PDE-GSH-adduct in HepG2-induced cells (MH^+, *m/z* 610). (C) Intracellular (±)-B[*a*]PDE-GSH-adducts in TCDD-induced HepG2 cells after a 4 h incubation.

of magnitude increase of both intracellular and extracellular B[*a*]PDE-GSH-adducts in the H358 lung cells (Figure 8A and B) when compared with that in HepG2 liver cells (Figure 8C and D). To confirm that these changes were a result of alterations in GSTs rather than modifications in GSH biosynthesis and utilization, the GSH/GSSG ratio was quantified by stable isotope dilution LC-MS (*27*). This ratio did not change significantly in H358 control cells versus TCDD-induced cells, and GSH concentrations did not change (Supporting Information, Figure 1).

GST Activity Assay. The overall activity of GSTs was assessed in TCDD-induced and noninduced H358 and HepG2 cells. The GST activity increased modestly in H358 cells treated with 10 nM TCDD for 24 h (Table 1). In contrast, the GST activity in HepG2 cells was slightly lower than that found in H358 cells and was further reduced by TCDD treatment (Table 1).

Discussion

DNA- and GSH-adduct formation was assessed in the H358 human bronchoalveolar cell line because they are known to have basal levels of CYPs and AKRs without induction and are a well-characterized cell model for B[*a*]P metabolism in the lung (*23*−*25, 28, 29*). Similar studies were conducted in the HepG2 cell line because it has previously been employed extensively as a model for B[*a*]P metabolism in the liver (*30*−*33*). Previous studies by our group showed that (+)-B[*a*]PDE-dGuo adducts were found in higher concentration in H358 parental cells not treated with TCDD to induce P450 expression than in the corresponding TCDD-induced cells (*4*). To confirm these data, we examined how the concentration of (−)-B[*a*]P-7,8-dihydrodiol affected the formation of (+)-B[*a*]PDE-dGuo in H358 cells. At both low and high concentrations of (−)-B[*a*]P-7,8-dihydrodiol, there was an increase in DNA-adducts formed in H358 cells when compared with that in TCDD-induced cells (Figure 1). The TCDD-induced cells metabolized the (−)-B[*a*]P-7,8-dihydrodiol more rapidly than the noninduced cells so that it could still be detected by LC-MRM/MS in the noninduced cells after a 6 h incubation (Figure 2). Furthermore, there was a dose−response in the ability of TCDD to reduce B[*a*]PDE-dGuo formation (Figure 3).

Data obtained in lung cells greatly contrasts with that obtained in liver cells, where there was a significant increase in DNA-adducts after TCDD treatment (*34*). The effect of TCDD has been ascribed to the up-regulation of P4501A1/1B1 (*35*−*38*). Therefore, our findings raised the intriguing possibility that TCDD-induction (*39*) is protective against (+)-B[*a*]PDE-mediated DNA damage in the lung even though P4501A1/1B1 are required for the activation of (−)-B[*a*]P-7,8-dihydrodiol to the ultimate genotoxin, (+)-B[*a*]PDE (*18, 20*).

In order to gain further insight into gene regulation, a microarray analysis was performed in H358 cells that had been treated with TCDD and or (−)-B[*a*]P-7,8-dihydrodiol. TCDD was found previously to induce 8 genes (CYP1A1, CYP1B1, CRYZ, GSTM1, GLRX, ALDH3, ALDH1A3, and ALDH10) in human A549 and HPL1A lung cells through the aryl hydrocarbon receptor (AhR) pathway (*40*). As was found with A549 and HPLA1 lung cells, CYP1A1 was the major gene that was up-regulated by TCDD in the H358 cells, followed by CYP1B1 (Figure 4). We found that there was also significant up-regulation of GSTM1, ALDH3A1, and ALDH1A3. However, in contrast to the A549 and HPLA1 cells (*40*), up-regulation of CRYZ, GLRX, ALDH10 was not detected in the H358 cells. TCDD binds to the AhR, a cytosolic, ligand activated transcription factor. The AhR is complexed with chaperone proteins, including p23, XAP2/ARA9, and Hsp90 (*41, 42*). When TCDD binds to the AhR, a conformational change occurs, which results in the loss of certain chaperone proteins and nuclear localization (*37*). Once the TCDD-bound AhR has translocated to the nucleus, it binds with the AhR nuclear translocater. This complex then binds to consensus nucleotide sequences, termed xenobiotic response elements (XREs), in the 5′ untranslated region of responsive genes and modulates the transcription of these genes.

Induction of P4501A1/1B1 by (−)-B[*a*]P-7,8-dihdyrodiol (Figure 4) most likely results through the formation of the planar metabolite B[*a*]P-7,8-dione formed in the AKR pathway (*23*). The expression of AKRs was not significantly (>2-fold) induced by TCDD or (−)-B[*a*]P-7,8-dihydrodiol cell treatments when compared with that of dimethylsulfoxide alone (data not shown). However, the microarray results revealed that mRNA for AKR1B1, 1A1, 1C1, 1C2, 7A2, and 7A3 was present in the cells (data not shown). We previously noted that there was a lag in the formation of (+)-B[*a*]PDE-dGuo adducts in H358 cells treated with B[*a*]P-7,8-dihydrodiol. Therefore, we suggest that B[*a*]P-7,8-dihydrodiol is converted to the B[*a*]P-7,8-catechol by a member of the AKR family. The catechol then undergoes a two-electron oxidation to form the planar B[*a*]P-7,8-dione, and it is most likely the metabolite to bind the AhR, thus

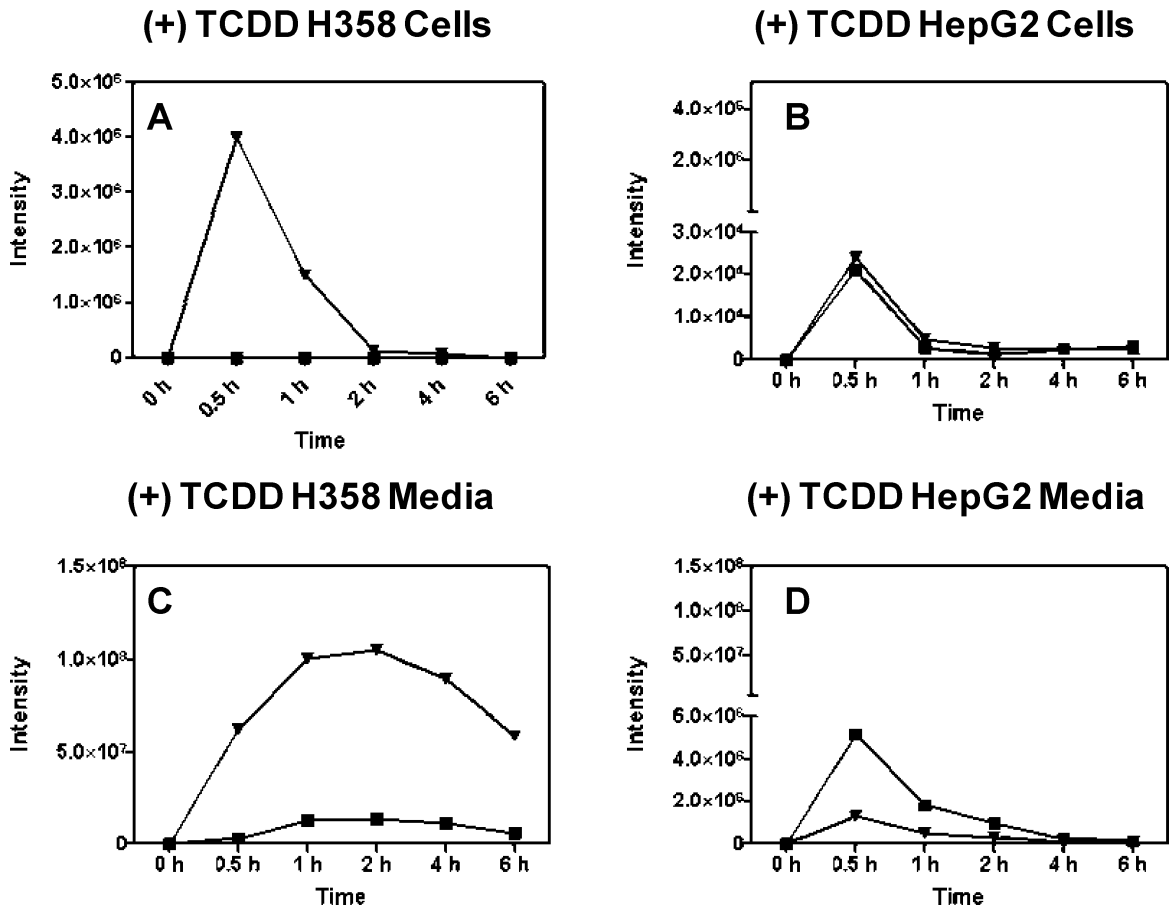

Figure 8. B[*a*]PDE-GSH-adducts in H358 and HepG2 cells and media after TCDD induction. H358 and HepG2 cells were treated with (±)-B[*a*]PDE for 30 min, 1, 2, 4, and 6 h with 10 nM TCDD pretreatment for 24 h and GSH-adducts quantified by LC-MS. (A) Intracellular (±)-B[*a*]PDE-GSH-adducts in H358 cells. (B) Intracellular (±)-B[*a*]PDE-GSH-adducts in HepG2 cells. (C) (±)-B[*a*]PDE-GSH-adducts in H358 cell media. (D) (±)-B[*a*]PDE-GSH-adducts in HepG2 cell media. Analyses were conducted in duplicate, and the mean values are shown. (−)-B[*a*]PDE-GSH-adduct (solid triangle); (+)-B[*a*]PDE-GSH-adduct (solid square).

inducing P450 expression through the pathway described above for TCDD. In order to confirm this protective effect, direct B[*a*]PDE-mediated DNA-adduct formation was examined in the TCDD-induced and noninduced H358 cells. This showed that (+)-B[*a*]PDE-dGuo adducts were significantly reduced in the TCDD-treated H358 cells when compared with those in the noninduced cells (Figure 5).

The most logical explanation for the TCDD effect on DNA-adduct formation is that increased metabolism of (+)-B[*a*]PDE had occurred. It has recently been recognized that TCDD can up-regulate GSTs in rodent cells (*43*). If this occurred in human lung cells, it could result in increased conversion of (+)-B[*a*]PDE to B[*a*]PDE-GSH-adducts, which would decrease the availability of (+)-B[*a*]PDE for DNA-adduct formation as shown in Scheme 2. In order to test this possibility, authentic (±)-B[*a*]PDE-GSH-adducts were prepared and their LC-MS characteristics determined. (±)-B[*a*]PDE-GSH-adduct formation was then determined in H358 and HepG2 cells and media with or without TCDD treatment. LC-MS/MS analysis revealed that the (−)-B[*a*]PDE-GSH-adduct was a significant metabolite in both TCDD-induced (Figure 6A) and noninduced H358 cells (Figure 6C). However, there was an almost a 10-fold increase in the (−)-B[*a*]PDE-GSH-adduct in TCDD-induced H358 cells (Figure 6A) when compared with that in the noninduced cells (Figure 6C). Formation of B[*a*]PDE-GSH-adducts in HepG2 cells (Figure 7C) also occurred, but levels were much lower than that in H358 cells (Figure 7A). GSH-adducts once secreted by cells are metabolized to their corresponding cysteinylglycine adducts by γ-glutamyltranspeptidase, which is localized on the external surface of the plasma membrane (*44, 45*). The loss of the initially formed B[*a*]P-GSH-adducts over time observed in the H358 and HepG2 cell media (Figures 8 and 9) is in keeping with this expected pathway of metabolism. However, the formation of the B[*a*]P-cysteinylglycine-adducts or their further dipeptidase and *N*-acetyl-cysteine-transferase-mediated conversion to cysteine (*45*) and *N*-acetylcysteine metabolites (*46*) was not monitored in the present study.

Analysis of HepG2 cells and media revealed the formation of the (±)-B[*a*]PDE-GSH-adduct rather than the (−)-enantiomer, suggesting that different GSTs are responsible for GSH-adduct formation in lung cells compared with that in liver cells. GSTπ, an abundant GST in the lung but not in hepatocytes (*47*), efficiently converts (+)-B[*a*]PDE into (−)-B[a]PDE-GSH (Scheme 1) (*26, 48, 49*). GSTα and GSTμ show much lower enantioselectivity for (+)-B[*a*]PDE, and in addition, GSTμ is primarily expressed in the liver rather than the lung (*50, 51*). Previous studies have shown that GSTπ-expressing cell lines are protected against (+)-B[*a*]PDE-mediated DNA damage (*52, 53*). Therefore, it is likely that GSTα and/or GSTμ are responsible for the racemic formation of B[*a*]PDE-GSH-adducts in the liver-derived HepG2 cells, whereas GSTπ is responsible for enantioselective GSH-adduct formation in the lung-derived H358 cells. Intracellular and extracellular (−)-B[*a*]PDE-GSH-adduct levels in our study were an order of magnitude higher in the TCDD-induced H358 lung cells (Figure 8A and B) when compared with that in the noninduced cells (Figure 9A and B), whereas TCDD induction (Figure 8C and D) had little effect on the HepG2 liver cells when compared with that in the

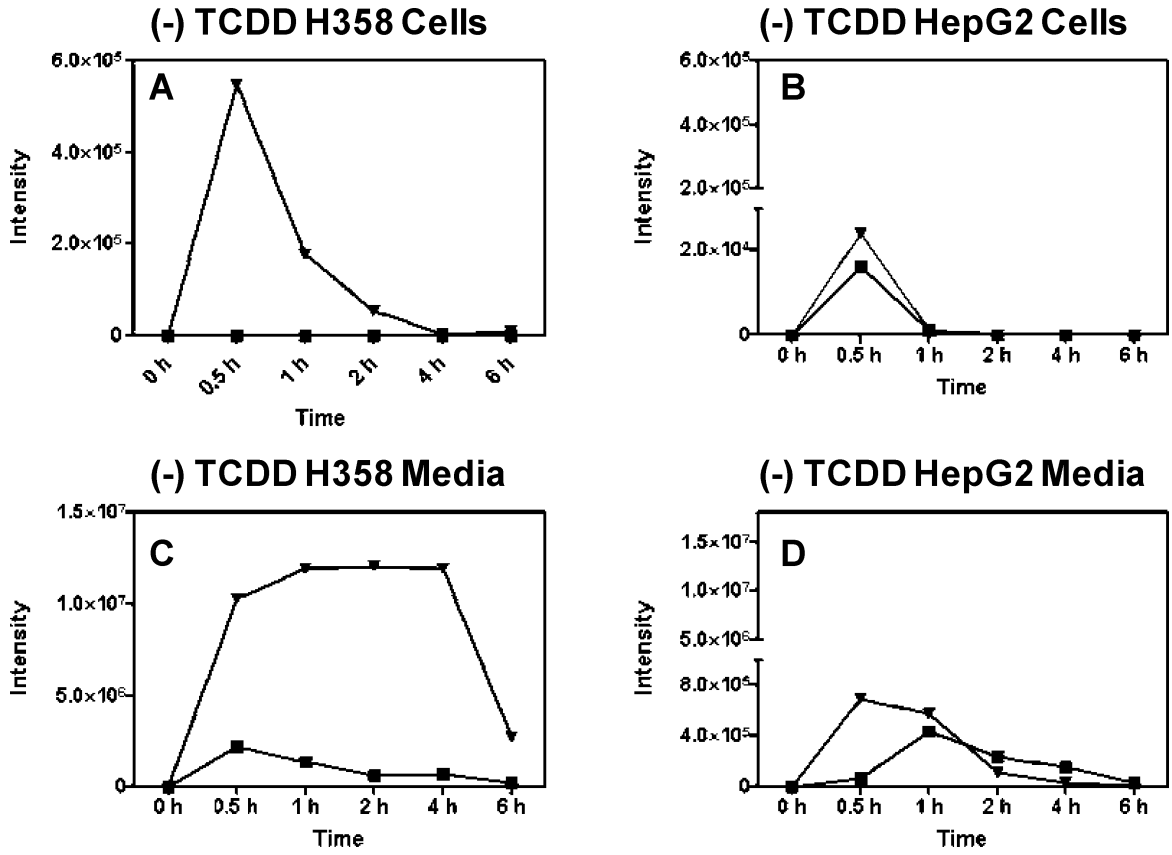

Figure 9. B[*a*]PDE-GSH-adducts in H358 and HepG2 cells and media with no TCDD induction. H358 and HepG2 cells were treated with (±)-B[*a*]PDE for 30 min, 1, 2, 4, and 6 h without TCDD pretreatment for 24 h and GSH-adduct formation quantified by LC-MS. (A) Intracellular (±)-B[*a*]PDE-GSH-adducts in H358 cells. (B) Intracellular (±)-B[*a*]PDE-GSH-adducts in HepG2 cells. (C) (±)-B[*a*]PDE-GSH-adducts in H358 cell media. (D) (±)-B[*a*]PDE-GSH-adducts HepG2 cell media. Analyses were conducted in duplicate, and the mean values are shown. (−)-B[*a*]PDE-GSH-adduct (solid triangle); (+)-B[*a*]PDE-GSH-adduct (solid square).

Table 1. GST Activity Levels in H358 and HepG2 Cells

cell samples	GST activity (nmol/min/mg protein)
H358 (−) TCDD	72026
H358 (+) TCDD	85238
HepG2 (−) TCDD	60637
HepG2 (+) TCDD	17679

noninduced cells (Figure 9C and D). Therefore, there was a stark contrast between the TCDD-induced H358 lung and HepG2 liver cells. Intracellular and extracellular (−)-B[*a*]PDE-GSH-adduct levels were almost 2 orders of magnitude higher in the TCDD-induced H358 cells (Figure 8A and B) when compared with the (±)-B[*a*]PDE-GSH-adduct levels in the induced HepG2 cells (Figure 8C and D).

These findings are consistent with lung cell specific TCDD-mediated up-regulation of GST isoforms that have enantioselectivity similar to that found for GSTπ-mediated detoxification of (+)-B[*a*]PDE (*26, 48, 49*) or induction of a post-translational modification that increases the activity of GSTπ. However, we were unable to detect up-regulation of any GSTs with the required stereoselectivity. It is noteworthy that GSTπ can undergo epidermal growth fact receptor-mediated phosphorylation at Tyrosine-7 and Tyrosine-198 (*54*). In addition, GSTπ is phosphorylated by the action of serine/threonine kinases, protein kinase C, and protein kinase A (*55*). Furthermore, epidermal growth fact receptor-mediated phosphorylation of Tyrosine-7 and Tyrosine-198 was found to increase the activity of GSTπ through a conformational change in the enzyme (*54*). Therefore, there is a body of literature to suggest that the substantial increase in GSH-adduct formation we observed could have arisen through a TCDD-mediated increase in the phosphorylation of GSTπ with a concomitant increase in its activity.

Scheme 2. Activation of B[*a*]P and Detoxification of the Resulting B[*a*]PDE in Human Lung Cells[a]

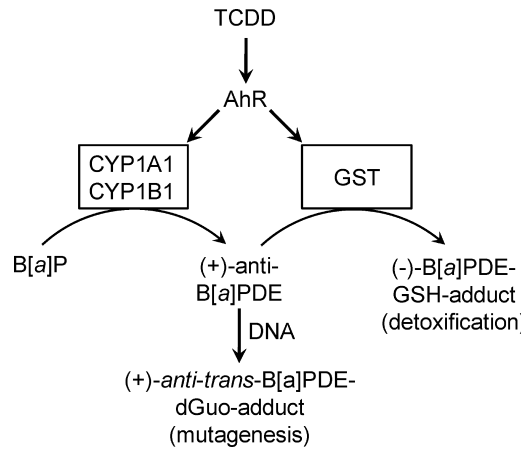

[a] TCDD induces P450s 1A1 and 1B1, which activate B[*a*]P to the reactive intermediate (+)-B[*a*]PDE in the lung. This either reacts with dGuo in DNA to form the (+)-B[*a*]PDE-dGuo adduct and initiates mutagenesis or is detoxified by GST to the (−)-B[*a*]PDE-GSH-adduct. TCDD induces P450s 1A1 and 1B1 through the AhR to increase the activation of B[*a*]P. It is proposed that there is another AhR-mediated interaction, which results in the increased expression of GSTs that can detoxify (+)-B[*a*]PDE with high enantioselectivity. A balance between the activation and detoxification pathways would then determine the amount of DNA damage that occurs.

Total GST activity was quantified using the CDNB conjugation assay to assess the level of all GSTs present in H358 and

HepG2 cells. The method was used previously to compare GST expression between lung and liver cells (*56*). A modest increase in total GST levels was observed in TCDD-induced H358 cells, whereas a significant decrease in GST activity was observed in TCDD-induced HepG2 cells (Table 1). Dostal et al. have reported that the highest affinity for CDNB is GSTα (*21*), further suggesting that this GST isoform is not an important mediator of B[*a*]PDE-GSH-adduct formation. It is noteworthy that a recent study was unable to detect any GSH-derived adducts of B[*a*]PDE in primary human hepatocytes (*46*). However, B[*a*]PDE-GSH-adducts were not analyzed directly, but the corresponding *N*-acetyl-cysteine-adducts were employed as surrogate biomarkers of GSH-adduct formation. The formation of *N*-acetylcysteine-adducts requires γ-glutamyltransferase-mediated conversion of the GSH-adducts into cysteinylglycine-adducts, followed by dipeptidase hydrolysis to the cysteine-adducts, and subsequent *N*-acetyl transferase-mediated acetylation (*45*). Therefore, it is conceivable that the resulting B[*a*]PDE-*N*-acetylcysteine-adducts were not formed in sufficient quantities by this complex metabolic pathway in order to permit their detection.

In summary, TCDD-induction of P4501A1/1B1 in lung cells would be predicted to increase the activation of (−)-B[*a*]P-7,8-dihydrodiol to (+)-B[*a*]PDE resulting in increased DNA damage when compared with noninduced cells. However, the TCDD was found to also up-regulate GST-mediated conversion of (+)-B[*a*]PDE to (−)-B[*a*]PDE-GSH-adducts. The increased formation of nongenotoxic GSH-adducts resulted in decreased amounts of (+)-B[*a*]PDE-mediated DNA damage in (±)-B[*a*]PDE-treated lung cells (Scheme 2). TCDD did not cause any changes in GSH or GSSG levels (Supporting Information, Figure 1). This suggests that the increased GSH-adduct formation most likely occurred through up-regulation of a GST with high enantioselectivity for (+)-B[*a*]PDE detoxification (*26, 48, 49*). Therefore, our data provide compelling evidence that TCDD can induce the metabolism of (+)-B[*a*]PDE to a nongenotoxic GSH-adduct in lung-derived H358 cells most likely through an AhR-dependent pathway (Scheme 2). It has been proposed that TCDD/AhR-mediated induction of antioxidant response element (ARE) driven genes such as GSTs can occur in rodent models through the Nrf2-Keap1 pathway (*43*). However, there is no evidence that human GSTs possess AREs in their noncoding region, and therefore, it seems unlikely that this mechanism can explain our findings. Unfortunately, the majority of GST induction studies have been conducted in rodent cells (*43, 57*), and therefore, the ability of TCDD to regulate the activity of GSTs in human cells will clearly require substantial additional studies. It will also be necessary to confirm that our findings can be observed in other human lung derived cells. However, to our knowledge, this is the first report that TCDD can induce GSH-adduct formation in human lung cells and therefore provides a useful model system with which to pursue further studies.

Acknowledgment. This project was supported by NIH grants 5F32ES016683, R01CA130038, R01ES015857, and P30ES013508.

Note Added after ASAP Publication. This paper was published on the Web on October 28, 2010, with an error in Figure 6. The corrected version was reposted on November 15, 2010.

Supporting Information Available: Determination of GSH/GSSG ratios by stable isotope dilution LC-MS. This material is available free of charge via the Internet at http://pubs.acs.org.

References

(1) Mastrangelo, G., Fadda, E., and Marzia, V. (1996) Polycyclic aromatic hydrocarbons and cancer in man. *Environ. Health Perspect. 104* (11), 1166–1170.
(2) Baird, W. M., Hooven, L. A., and Mahadevan, B. (2005) Carcinogenic polycyclic aromatic hydrocarbon-DNA adducts and mechanism of action. *Environ. Mol. Mutagen. 45* (2−3), 106–114.
(3) Hecht, S. S. (2006) Cigarette smoking: cancer risks, carcinogens, and mechanisms. *Langenbecks Arch. Surg. 391* (6), 603–613.
(4) Ruan, Q., Gelhaus, S. L., Penning, T. M., Harvey, R. G., and Blair, I. A. (2007) Aldo-keto reductase- and cytochrome P450-dependent formation of benzo[*a*]pyrene-derived DNA-adducts in human bronchoalveolar cells. *Chem. Res. Toxicol. 20* (3), 424–431.
(5) Castano-Vinyals, G., D'Errico, A., Malats, N., and Kogevinas, M. (2004) Biomarkers of exposure to polycyclic aromatic hydrocarbons from environmental air pollution. *Occup. Environ. Med. 61* (4), e12.
(6) IARC. (1983) Polynuclear aromatic compounds. Part 1. Chemical, environmental, and experimental data. *Monogr. Eval. Carcinogen. Risks Humans 32*, 1–477.
(7) Gelboin, H. V. (1980) Benzo[alpha]pyrene metabolism, activation and carcinogenesis: role and regulation of mixed-function oxidases and related enzymes. *Physiol. Rev. 60* (4), 1107–1166.
(8) Xue, W., and Warshawsky, D. (2005) Metabolic activation of polycyclic and heterocyclic aromatic hydrocarbons and DNA damage: a review. *Toxicol. Appl. Pharmacol. 206* (1), 73–93.
(9) Wogan, G. N., Hecht, S. S., Felton, J. S., Conney, A. H., and Loeb, L. A. (2004) Environmental and chemical carcinogenesis. *Semin. Cancer Biol. 14* (6), 473–486.
(10) Shimada, T. (2006) Xenobiotic-metabolizing enzymes involved in activation and detoxification of carcinogenic polycyclic aromatic hydrocarbons. *Drug Metab. Pharmacokinet. 21* (4), 257–276.
(11) Srivastava, S. K., Watkins, S. C., Schuetz, E., and Singh, S. V. (2002) Role of glutathione conjugate efflux in cellular protection against benzo[a]pyrene-7,8-diol-9,10-epoxide-induced DNA damage. *Mol. Carcinog. 33* (3), 156–162.
(12) Mangal, D., Vudathala, D. K., Park, J. H., Lee, S. H., Penning, T. M., and Blair, I. A. (2009) Analysis of 7,8-Dihydro-8-oxo-2′-deoxyguanosine in cellular DNA during oxidative stress. *Chem. Res. Toxicol. 22* (5), 788–797.
(13) Armstrong, B., Hutchinson, E., Unwin, J., and Fletcher, T. (2004) Lung cancer risk after exposure to polycyclic aromatic hydrocarbons: a review and meta-analysis. *Environ. Health Perspect. 112* (9), 970–978.
(14) Pfeifer, G. P., Denissenko, M. F., Olivier, M., Tretyakova, N., Hecht, S. S., and Hainaut, P. (2002) Tobacco smoke carcinogens, DNA damage and p53 mutations in smoking-associated cancers. *Oncogene 21* (48), 7435–7451.
(15) Boffetta, P., Jourenkova, N., and Gustavsson, P. (1997) Cancer risk from occupational and environmental exposure to polycyclic aromatic hydrocarbons. *Cancer Causes Control 8* (3), 444–472.
(16) Rubin, H. (2001) Synergistic mechanisms in carcinogenesis by polycyclic aromatic hydrocarbons and by tobacco smoke: a bio-historical perspective with updates. *Carcinogenesis 22* (12), 1903–1930.
(17) Denissenko, M. F., Pao, A., Tang, M., and Pfeifer, G. P. (1996) Preferential formation of benzo[a]pyrene adducts at lung cancer mutational hotspots in P53. *Science 274* (5286), 430–432.
(18) Shimada, T., Gillam, E. M., Oda, Y., Tsumura, F., Sutter, T. R., Guengerich, F. P., and Inoue, K. (1999) Metabolism of benzo[a]pyrene to trans-7,8-dihydroxy-7, 8-dihydrobenzo[a]pyrene by recombinant human cytochrome P450 1B1 and purified liver epoxide hydrolase. *Chem. Res. Toxicol. 12* (7), 623–629.
(19) Shimada, T., Oda, Y., Gillam, E. M., Guengerich, F. P., and Inoue, K. (2001) Metabolic activation of polycyclic aromatic hydrocarbons and other procarcinogens by cytochromes P450 1A1 and P450 1B1 allelic variants and other human cytochromes P450 in *Salmonella typhimurium* NM2009. *Drug Metab. Dispos. 29* (9), 1176–1182.
(20) Shimada, T., and Fujii-Kuriyama, Y. (2004) Metabolic activation of polycyclic aromatic hydrocarbons to carcinogens by cytochromes P450 1A1 and 1B1. *Cancer Sci. 95* (1), 1–6.
(21) Dostal, L. A., Guthenberg, C., Mannervik, B., and Bend, J. R. (1988) Stereoselectivity and regioselectivity of purified human glutathione transferases pi, alpha-epsilon, and mu with alkene and polycyclic arene oxide substrates. *Drug Metab. Dispos. 16* (3), 420–424.
(22) Singh, S. V., Varma, V., Zimniak, P., Srivastava, S. K., Marynowski, S. W., Desai, D., Amin, S., and Ji, X. (2004) Structural basis for catalytic differences between alpha class human glutathione trans-

ferases hGSTA1-1 and hGSTA2-2 for glutathione conjugation of environmental carcinogen benzo[a]pyrene-7,8-diol-9,10-epoxide. *Biochemistry 43* (30), 9708–9715.
(23) Jiang, H., Vudathala, D. K., Blair, I. A., and Penning, T. M. (2006) Competing roles of aldo-keto reductase 1A1 and cytochrome P4501B1 in benzo[a]pyrene-7,8-diol activation in human bronchoalveolar H358 cells: role of AKRs in P4501B1 induction. *Chem. Res. Toxicol. 19* (1), 68–78.
(24) Ruan, Q., Kim, H. Y., Jiang, H., Penning, T. M., Harvey, R. G., and Blair, I. A. (2006) Quantification of benzo[a]pyrene diol epoxide DNA-adducts by stable isotope dilution liquid chromatography/tandem mass spectrometry. *Rapid Commun. Mass Spectrom. 20* (8), 1369–1380.
(25) Jiang, H., Gelhaus, S. L., Mangal, D., Harvey, R. G., Blair, I. A., and Penning, T. M. (2007) Metabolism of benzo[a]pyrene in human bronchoalveolar H358 cells using liquid chromatography-mass spectrometry. *Chem. Res. Toxicol. 20* (9), 1331–1341.
(26) Srivastava, S. K., Hu, X., Xia, H., Bleicher, R. J., Zaren, H. A., Orchard, J. L., Awasthi, S., and Singh, S. V. (1998) ATP-dependent transport of glutathione conjugate of 7beta, 8alpha-dihydroxy-9alpha,10alpha-oxy-7,8,9,10-tetrahydrobenzo[a]pyrene in murine hepatic canalicular plasma membrane vesicles. *Biochem. J. 332* (Pt. 3), 799–805.
(27) Zhu, P., Oe, T., and Blair, I. A. (2008) Determination of cellular redox status by stable isotope dilution liquid chromatography/mass spectrometry analysis of glutathione and glutathione disulfide. *Rapid Commun. Mass Spectrom. 22* (4), 432–440.
(28) Jiang, H., Shen, Y. M., Quinn, A. M., and Penning, T. M. (2005) Competing roles of cytochrome P450 1A1/1B1 and aldo-keto reductase 1A1 in the metabolic activation of (±)-7,8-dihydroxy-7,8-dihydrobenzo[a]pyrene in human bronchoalveolar cell extracts. *Chem. Res. Toxicol. 18* (2), 365–374.
(29) Caino, M. C., Oliva, J. L., Jiang, H., Penning, T. M., and Kazanietz, M. G. (2007) Benzo[a]pyrene-7,8-dihydrodiol promotes checkpoint activation and G2/M arrest in human bronchoalveolar carcinoma H358 cells. *Mol. Pharmacol. 71* (3), 744–750.
(30) Hockley, S. L., Arlt, V. M., Brewer, D., Te, P. R., Workman, P., Giddings, I., and Phillips, D. H. (2007) AHR- and DNA-damage-mediated gene expression responses induced by benzo(a)pyrene in human cell lines. *Chem. Res. Toxicol. 20* (12), 1797–1810.
(31) Mattsson, A., Lundstedt, S., and Stenius, U. (2009) Exposure of HepG2 cells to low levels of PAH-containing extracts from contaminated soils results in unpredictable genotoxic stress responses. *Environ. Mol. Mutagen. 50* (4), 337–348.
(32) Naspinski, C., Gu, X., Zhou, G. D., Mertens-Talcott, S. U., Donnelly, K. C., and Tian, Y. (2008) Pregnane X receptor protects HepG2 cells from BaP-induced DNA damage. *Toxicol. Sci. 104* (1), 67–73.
(33) Wei, W., Zhang, C., Liu, A. L., Xie, S. H., Chen, X. M., and Lu, W. Q. (2009) Effect of PCB153 on BaP-induced genotoxicity in HepG2 cells via modulation of metabolic enzymes. *Mutat. Res. 675* (1−2), 71–76.
(34) Conney, A. H. (1982) Induction of microsomal enzymes by foreign chemicals and carcinogenesis by polycyclic aromatic hydrocarbons: G. H. A. Clowes Memorial Lecture. *Cancer Res. 42* (12), 4875–4917.
(35) Whitlock, J. P., Jr. (1999) Induction of cytochrome P4501A1. *Annu. Rev. Pharmacol. Toxicol. 39*, 103–125.
(36) Tijet, N., Boutros, P. C., Moffat, I. D., Okey, A. B., Tuomisto, J., and Pohjanvirta, R. (2006) Aryl hydrocarbon receptor regulates distinct dioxin-dependent and dioxin-independent gene batteries. *Mol. Pharmacol. 69* (1), 140–153.
(37) Taylor, R. T., Wang, F., Hsu, E. L., and Hankinson, O. (2009) Roles of coactivator proteins in dioxin induction of CYP1A1 and CYP1B1 in human breast cancer cells. *Toxicol. Sci. 107* (1), 1–8.
(38) Kim, S., Dere, E., Burgoon, L. D., Chang, C. C., and Zacharewski, T. R. (2009) Comparative analysis of AhR-mediated TCDD-elicited gene expression in human liver adult stem cells. *Toxicol. Sci. 112* (1), 229–244.
(39) Nebert, D. W., Dalton, T. P., Okey, A. B., and Gonzalez, F. J. (2004) Role of aryl hydrocarbon receptor-mediated induction of the CYP1 enzymes in environmental toxicity and cancer. *J. Biol. Chem. 279* (23), 23847–23850.
(40) Martinez, J. M., Afshari, C. A., Bushel, P. R., Masuda, A., Takahashi, T., and Walker, N. J. (2002) Differential toxicogenomic responses to 2,3,7,8-tetrachlorodibenzo-p-dioxin in malignant and nonmalignant human airway epithelial cells. *Toxicol. Sci. 69* (2), 409–423.
(41) Meyer, B. K., Pray-Grant, M. G., Vanden Heuvel, J. P., and Perdew, G. H. (1998) Hepatitis B virus X-associated protein 2 is a subunit of the unliganded aryl hydrocarbon receptor core complex and exhibits transcriptional enhancer activity. *Mol. Cell. Biol. 18* (2), 978–988.
(42) Petrulis, J. R., and Perdew, G. H. (2002) The role of chaperone proteins in the aryl hydrocarbon receptor core complex. *Chem.-Biol. Interact. 141* (1−2), 25–40.
(43) Yeager, R. L., Reisman, S. A., Aleksunes, L. M., and Klaassen, C. D. (2009) Introducing the 'TCDD Inducible AhR-Nrf2 Gene Battery'. *Toxicol. Sci.* xxxx.
(44) Pompella, A., De, T. V, Paolicchi, A., and Zunino, F. (2006) Expression of gamma-glutamyltransferase in cancer cells and its significance in drug resistance. *Biochem. Pharmacol. 71* (3), 231–238.
(45) Blair, I. A. (2010) Analysis of endogenous glutathione-adducts and their metabolites. *Biomed. Chromatogr. 24* (1), 29–38.
(46) Upadhyaya, P., Hochalter, J. B., Balbo, S., McIntee, E. J., and Hecht, S. S. (2010) Preferential glutathione conjugation of a reverse diol epoxide compared with a bay region diol epoxide of benzo[a]pyrene in human hepatocytes. *Drug Metab. Dispos. 38* (9), 1397–1402.
(47) Terrier, P., Townsend, A. J., Coindre, J. M., Triche, T. J., and Cowan, K. H. (1990) An immunohistochemical study of pi class glutathione S-transferase expression in normal human tissue. *Am. J. Pathol. 137* (4), 845–853.
(48) Hu, X., O'Donnell, R., Srivastava, S. K., Xia, H., Zimniak, P., Nanduri, B., Bleicher, R. J., Awasthi, S., Awasthi, Y. C., Ji, X., and Singh, S. V. (1997) Active site architecture of polymorphic forms of human glutathione S-transferase P1−1 accounts for their enantioselectivity and disparate activity in the glutathione conjugation of 7beta,8alpha-dihydroxy-9alpha,10alpha-oxy-7,8,9,10-tetrahydrobenzo(a)pyrene. *Biochem. Biophys. Res. Commun. 235* (2), 424–428.
(49) Sundberg, K., Johansson, A. S., Stenberg, G., Widersten, M., Seidel, A., Mannervik, B., and Jernstrom, B. (1998) Differences in the catalytic efficiencies of allelic variants of glutathione transferase P1−1 towards carcinogenic diol epoxides of polycyclic aromatic hydrocarbons. *Carcinogenesis 19* (3), 433–436.
(50) Robertson, I. G., Guthenberg, C., Mannervik, B., and Jernstrom, B. (1986) Differences in stereoselectivity and catalytic efficiency of three human glutathione transferases in the conjugation of glutathione with 7 beta,8 alpha-dihydroxy-9 alpha,10 alpha-oxy-7,8,9,10-tetrahydrobenzo(a)pyrene. *Cancer Res. 46* (5), 2220–2224.
(51) Sundberg, K., Widersten, M., Seidel, A., Mannervik, B., and Jernstrom, B. (1997) Glutathione conjugation of bay- and fjord-region diol epoxides of polycyclic aromatic hydrocarbons by glutathione transferases M1−1 and P1−1. *Chem. Res. Toxicol. 10* (11), 1221–1227.
(52) Fields, W. R., Morrow, C. S., Doss, A. J., Sundberg, K., Jernstrom, B., and Townsend, A. J. (1998) Overexpression of stably transfected human glutathione S-transferase P1−1 protects against DNA damage by benzo[a]pyrene diol-epoxide in human T47D cells. *Mol. Pharmacol. 54* (2), 298–304.
(53) Sundberg, K., Dreij, K., Seidel, A., and Jernstrom, B. (2002) Glutathione conjugation and DNA adduct formation of dibenzo[a,l]pyrene and benzo[a]pyrene diol epoxides in V79 cells stably expressing different human glutathione transferases. *Chem. Res. Toxicol. 15* (2), 170–179.
(54) Okamura, T., Singh, S., Buolamwini, J., Haystead, T., Friedman, H., Bigner, D., and Ali-Osman, F. (2009) Tyrosine phosphorylation of the human glutathione S-transferase P1 by epidermal growth factor receptor. *J. Biol. Chem. 284* (25), 16979–16989.
(55) Lo, H. W., Antoun, G. R., and Ali-Osman, F. (2004) The human glutathione S-transferase P1 protein is phosphorylated and its metabolic function enhanced by the Ser/Thr protein kinases, cAMP-dependent protein kinase and protein kinase C, in glioblastoma cells. *Cancer Res. 64* (24), 9131–9138.
(56) Pushparajah, D. S., Umachandran, M., Plant, K. E., Plant, N., and Ioannides, C. (2008) Up-regulation of the glutathione S-transferase system in human liver by polycyclic aromatic hydrocarbons; comparison with rat liver and lung. *Mutagenesis 23* (4), 299–308.
(57) Hayes, J. D., Flanagan, J. U., and Jowsey, I. R. (2005) Glutathione transferases. *Annu. Rev. Pharmacol. Toxicol. 45*, 51–88.

TX100297Z